ELSEVIER

Chemical Geology 235 (2006) 21–32

CHEMICAL GEOLOGY
INCLUDING
ISOTOPE GEOSCIENCE

www.elsevier.com/locate/chemgeo

U–Pb dating of perovskite by LA-ICP-MS: An example from the Oka carbonatite, Quebec, Canada

Richard A. Cox [a,*], Derek H.C. Wilton [b]

[a] Université du Québec a Chicoutimi, Dept. des Sciences Appliquees, Chicoutimi, QC, Canada, G7H 2B1
[b] Memorial University of Newfoundland, Department of Earth Sciences, St. John's, NL, Canada, A1B 3X5

Received 22 July 2004; received in revised form 26 May 2006; accepted 2 June 2006

Editor: R.L. Rudnick

Abstract

The potential for U–Pb dating of the mineral perovskite, using laser ablation inductively coupled plasma-mass spectrometry (LA-ICP-MS), has been evaluated. Perovskite can have relatively elevated U and Th contents, making it a potentially useful geochronometer. Kimberlite, lamprophyre and carbonatite intrusions are prone to alteration and typically contain abundant xenocrysts, thus standard techniques for dating the magmatic emplacement of these rocks becomes highly problematic. Perovskite, however, is commonly present as a primary magmatic mineral in these rocks and has been used to constrain the timing of kimberlite and lamprophyre emplacement. The main limitations to the production of accurate LA-ICP-MS U–Pb ages for perovskite are the lack of suitable standards coupled with the large common-Pb correction required. ^{204}Hg can produce large isobaric interference on the non-radiogenic ^{204}Pb isotope and methods based on ^{208}Pb/^{206}Pb and U/Th ratios are hampered by the enhanced Th content present in most perovskite crystals. After careful calibration using zircon reference materials, common-Pb corrected ^{206}Pb/^{238}U ages can be determined on each individual LA-ICP-MS analysis by using the measured ^{207}Pb/^{206}Pb ratio which is dominated by the common-Pb proportion in phanerozoic rocks. This method assumes that the perovskite crystals analyzed are cogenetic and have the same initial-Pb ratios. The LA-ICP-MS method has been applied to data collected on two large, single perovskite crystals from the Oka carbonatite complex, Quebec, Canada. The weighted mean ^{206}Pb/^{238}U age of 131+/−7 Ma (N=25, MSWD=0.42) is consistent with published geochronology data from the region and suggests that LA-ICP-MS dating of perovskite could be a useful, low-cost alternative to compliment existing techniques.

Keywords: Perovskite; LA-ICP-MS; U–Pb geochronology; Common-Pb corrections

1. Introduction

Rapid, low-cost dating utilizing the enhanced special resolution of a laser ablation microprobe attached to an inductively coupled plasma mass spectrometer (LA-ICP-MS) has developed rapidly from relatively simple determinations of radiogenic ^{207}Pb/^{206}Pb ratios (Feng et al., 1993; Fryer et al., 1993) to progressively more accurate and precise U–Pb and Th–Pb dating (e.g. Horn et al., 2000; Li et al., 2001; Machado and Simonetti, 2001; Kosler et al., 2002). Applications range from investigation of detrital zircon ages (Machado and Gauthier, 1996; Scott, 1999; White et al., 2001) to the dating of accessory minerals in metamorphic and igneous rocks (Ballard et al., 2001; Foster et al., 2002; Hodych et al., 2004). The LA-ICP-MS technique has been mainly applied to dating the minerals

* Corresponding author. Tel.: +1 418 545 5011x2577; fax: +1 418 545 5012.
E-mail address: rcox@uqac.ca (R.A. Cox).

0009-2541/$ - see front matter © 2006 Elsevier B.V. All rights reserved.
doi:10.1016/j.chemgeo.2006.06.002

zircon and monazite, although it has also been successfully applied to dating titanite and allanite (Willigers et al., 2002; Cox et al., 2003).

Dating of kimberlite and lamprophyre has been conducted using magmatic mineral phases such as phlogopite and biotite (*via* K–Ar, Ar–Ar and Rb–Sr methods), zircon, baddeleyite and rutile (*via* U–Pb method). Such age-data are commonly interpreted as recording the timing of emplacement (Davis and Kjarsgaard, 1997; Armstrong and Moore, 1998; Phillips et al., 1998; Schmitz and Bowring, 2001; Heaman et al., 2002). Determinations of precise emplacement ages for kimberlite and lamprophyre, however, are complicated due to the severe alteration which is commonly associated with these intrusions and the presence of xenocrysts which lead to disturbed, mixed and older, non-emplacement (inheritance) ages (e.g. Smith et al., 1994; Schaerer et al., 1997; Kelley and Wartho, 2000). Indeed, the tendency for kimberlite diatremes to concentrate a wide variety of different xenoliths has been exploited as a means of examining the composition and evolution of the rocks underlying cratonic terranes (Davis, 1997; Schmitz and Bowring, 2001; Heaman et al., 2002).

Perovskite ($CaTiSiO_3$) occurs as a magmatic matrix component in many mantle-derived mafic and ultramafic diatremes, dykes and small intrusions, and in alkaline igneous rocks as well as carbonatites where it may be present as large phenocrysts. As perovskite has not been shown to record inheritance, it has proven a useful mineral for dating the emplacement of kimberlite and lamprophyre intrusions mainly using conventional isotope dilution methods and sensitive high-resolution ion-microprobe or SHRIMP analyses (e.g. Queen et al., 1996; Kinney et al., 1997; Leckie et al., 1997; Heaman and Kjarsgaard, 2000). Given the economic importance of the rock-types commonly containing perovskite, the potential to date the emplacement ages of these rocks using the rapid and inexpensive LA-ICP-MS technique should be of considerable interest.

LA-ICP-MS U–Pb dating has already been applied to zircon from kimberlite intrusions (Belousova et al., 2001; Spetsius et al., 2002). Perovskite however, presents additional problems, primarily associated with common-Pb corrections and high-Th contents, which need to be overcome before accurate LA-ICP-MS can be determined. In this study we have used LA-ICP-MS U–Pb dating to determine the ages of two large perovskite crystals from the Oka carbonatite, near Montreal, Canada in order to test the effectiveness of the method applied to this mineral. The samples formed part of the Steve Papesic mineral collection at Memorial University of Newfoundland. The location of the samples was elucidated following a number of visits to the Oka region. The perovskite crystals used in this study formed part of the olivine–monticellite–sövite series of rocks found in the Bond zone in the southern part of the intrusion (Gold et al., 1986). These rocks are thought to be among the earliest of the complex to be emplaced into fenitzed Precambrian country rocks (Gold et al., 1986).

2. U–Th–Pb LAM-ICP-MS dating of perovskite

2.1. General method

In-situ LA-ICP-MS analyses of areas within the selected zircon reference materials and two large (0.5 cm) euhedral, cubes of perovskite from the Oka Complex were carried out using a VG PlasmaQuad PQ-2S+ instrument coupled to an in-house 266 nm NdYAG laser at Memorial University of Newfoundland. The method follows that of Kosler et al. (2002) and Cox et al. (2003). The sample introduction system has been modified to enable nebulization of a tracer solution at the same time as laser ablation of the solid sample. In this study we used a mixed tracer solution of ^{203}Tl–^{205}Tl–^{209}Bi–^{233}U–^{237}Np with 10 ppb of each element. The tracer solution was aspirated with an argon carrier gas into the plasma using a MCN-100 Cetac micro-concentric nebuliser, Scott-type double-pass spray chamber and a T-piece tube attached to the back end of the plasma torch. Solution sensitivities varied from around 30,000 cps/ppb for Tl and Bi to 60,000 cps/ppb for U and 12,000 cps/ppb for Np. Helium was used as the carrier gas mixture through a gas line (also attached to the T-piece tube) which carried the ablated sample from the laser cell (50 cm^3) to the plasma. The sample cell holds two 7 mm rounds, which held the reference zircons, and two 2.54 cm diameter mounts with the two, polished pervoskite crystals.

The laser was set up to produce 10–20 μm diameter spots with 0.25–0.8 mJ/pulse for the reference zircon analyses. The energy was kept at 0.5 mJ/pulse for all analysis of the Oka perovskite and a repetition rate of 10 Hz was used for all analyses. The laser beam was focused 100–200 μm above the sample surface. The cell is mounted to a motorized stage, which during ablation, was moved beneath the stationary laser beam to produce square and rectangular raster shapes. This provides a large enough area to slow the depth of the ablation without severely affecting special resolution. Previous studies have demonstrated that both laser beam defocus and rastering result in a more efficient removal of analyte from the ablation site and substantially reduce elemental fractionation between U, Th and Pb (Li et al., 2001; White et al., 2001). Typical acquisitions consisted of a 40 s measurement of gas blank and aspirated solution

Table 1
LA-ICP-MS data for MUN 02123 and Mt. Ste. Hilliare zircon reference materials

Analysis #	Laser conditions			Calculated ratios and common Pb content										Apparent ages (Ma)			
	LAM power (mJ/pulse)	Spot size (μm)	Raster size (μm × μm)	Th/U	$^{208}Pb/^{206}Pb$	f206%	$^{207}Pb/^{235}U$	+/−	$^{206}Pb/^{238}U$	+/−	$^{207}Pb/^{206}Pb$	+/−		$^{207}Pb/^{235}U$	+/−	$^{206}Pb/^{238}U$	+/−
MUN 02123																	
mr27a01 1	0.6	15	60×45	0.564	0.177	0.62	0.3312	0.0263	0.0478	0.0022	0.0503	0.0041		290	20	301	13
mr27a02 1	0.6	15	60×45	0.539	0.169	0.61	0.3264	0.0215	0.0460	0.0021	0.0515	0.0036		287	16	290	13
mr15c05 1	0.25	20	80×30	0.522	0.164	1.05	0.3453	0.0125	0.0465	0.0010	0.0509	0.0019		301	9	293	6
mr15c06 1	0.25	20	80×30	0.604	0.190	0.73	0.3577	0.0137	0.0460	0.0012	0.0502	0.0017		311	10	290	7
mr15c11 1	0.25	20	80×30	0.443	0.139	0.87	0.3737	0.0145	0.0459	0.0010	0.0561	0.0023		322	11	289	6
mr15c12 1	0.25	20	80×30	0.438	0.137	0.54	0.3230	0.0152	0.0472	0.0012	0.0478	0.0022		284	12	297	7
mr30a01 1	0.5	15	100×80	0.717	0.216	0.03	0.3456	0.0153	0.0452	0.0015	0.0558	0.0031		301	12	285	9
mr30a02 1	0.5	15	100×80	0.616	0.191	0.23	0.3446	0.0578	0.0467	0.0038	0.0535	0.0103		301	44	294	24
mr30a03 1	0.5	15	100×80	0.940	0.283	1.44	0.3175	0.0196	0.0468	0.0015	0.0485	0.0031		280	15	295	9
mr30a04 1	0.5	15	100×80	0.710	0.214	1.53	0.3326	0.0179	0.0460	0.0021	0.0506	0.0030		292	14	290	13
ap02a01 1	0.5	20	40×40	0.836	0.252	1.03	0.3232	0.0123	0.0453	0.0012	0.0502	0.0016		284	9	286	7
ap02a02 1	0.5	20	40×40	0.613	0.185	0.41	0.3158	0.0168	0.0463	0.0015	0.0486	0.0021		279	13	292	9
ap02a03 1	0.5	20	40×40	0.379	0.114	0.16	0.3189	0.0140	0.0455	0.0015	0.0485	0.0020		281	11	287	9
ap02a10 1	0.5	20	60×60	0.487	0.147	0.96	0.3655	0.0233	0.0481	0.0014	0.0530	0.0034		316	17	303	8
ap02a19 1	0.5	10	60×60	0.779	0.235	1.31	0.3296	0.0084	0.0472	0.0009	0.0504	0.0013		289	6	297	5
ap02a20 1	0.5	10	60×60	0.511	0.154	0.44	0.3073	0.0116	0.0440	0.0009	0.0494	0.0017		272	9	277	6
Mt.Ste.Hillaire																	
mr15c01 1	0.25	20	80×30	3.320	1.045	2.04	0.1390	0.0361	0.0206	0.0038	0.0489	0.0129		132	32	132	24
mr15c02 1	0.25	20	80×30	2.995	0.955	0.40	0.1425	0.0141	0.0212	0.0013	0.0487	0.0053		135	13	135	8
mr15c03 1	0.25	20	80×30	3.012	0.958	0.28	0.1568	0.0113	0.0230	0.0013	0.0494	0.0043		148	10	147	8
mr15c04 1	0.25	20	80×30	3.996	1.265	1.66	0.1342	0.0178	0.0196	0.0029	0.0497	0.0068		128	16	125	18
mr27a05 1	0.6	15	60×45	2.404	0.761	0.18	0.1427	0.0096	0.0216	0.0012	0.0479	0.0035		135	9	138	8
mr27a06 1	0.6	15	60×45	2.530	0.801	0.87	0.1494	0.0121	0.0228	0.0009	0.0476	0.0045		141	11	145	6
mr27a07 1	0.5	15	60×45	2.590	0.820	0.51	0.1559	0.0161	0.0229	0.0013	0.0493	0.0063		147	14	146	8
mr27a08 1	0.5	15	60×45	2.694	0.852	1.45	0.1693	0.0160	0.0246	0.0015	0.0500	0.0058		159	14	157	9
mr27a10 1	0.5	15	60×45	2.694	0.853	1.13	0.1582	0.0129	0.0241	0.0019	0.0476	0.0045		149	11	154	12
mr27a11 1	0.4	15	60×45	1.875	0.594	0.12	0.1434	0.0106	0.0202	0.0009	0.0515	0.0040		136	9	129	6

All errors and apparent ages quoted at the 1σ level.

prior to the start of ablation. During ablation, Pb, Th and U signals from the sample along with the continuous signals from the aspirated solution, were acquired for 200 s. The data were acquired in time resolved–peak jumping–pulse counting mode with 1 point measured per peak for masses 202 (Hg-flyback), 203 (Tl), 205 (Tl), 206 (Pb), 207 (Pb), 208 (Pb), 209 (Bi), 232 (Th), 233 (U), 237 (Np), 238 (U), 248 ($^{232}Th^{16}O$), 249 ($^{233}U^{16}O$), 253 ($^{237}Np^{16}O$) and 254 ($^{238}U^{16}O$). Quadrupole settling time was 1 ms and the dwell time was 8.3 ms on each mass except for ^{208}Pb (16.6 ms) and ^{207}Pb (24.9 ms). Over 200 s of measurement, around 1200 data acquisition cycles (sweeps) were collected.

2.2. Data reduction

Raw data were corrected for electron multiplier dead time (20 ns) and processed offline using an Excel spreadsheet program (LAMdate) to integrate signals from each sequential set of 10 sweeps. The measured counts are corrected for gas blank and the U, Th and Np signals are corrected for minor oxide formation before the correction for instrument mass bias. The mass bias correction utilized the power law and the ratio measurements of isotopic tracer solution. There is currently no commonly used perovskite reference material. To monitor the efficiency of the mass bias correction and residual laser induced fractionation repeat measurements of two zircon reference samples, 01232 (Ketchum et al., 2001) and an in-house zircon from Mt. Ste Hilliare were performed at regular intervals during each analytical session. Residual laser induced fractionation was between 0.05%/AMU and 0.25%/AMU during the 200 s laser analysis and is therefore small enough to be corrected using the linear intercept method (Kosler et al., 2002). Correcting the Pb-isotope signals from the zircon for initial common-Pb is problematic. Firstly, the amount of common-Pb in zircon is extremely small and secondly, ^{204}Hg

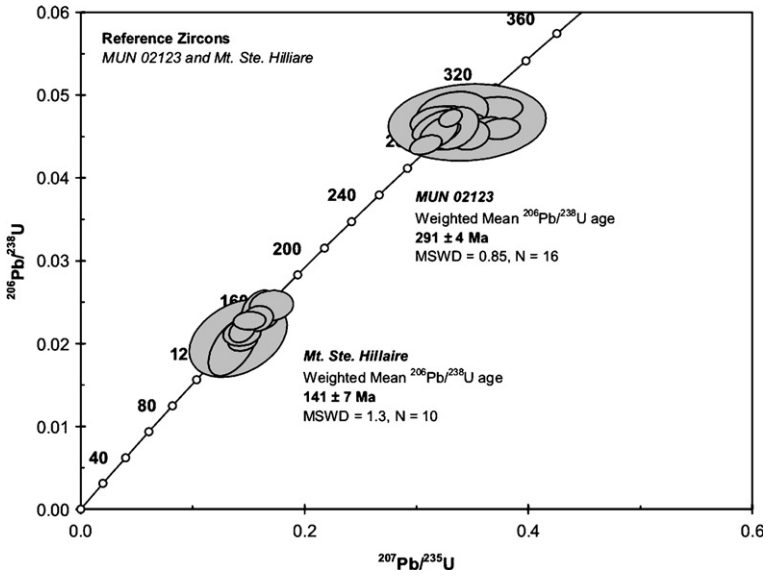

Fig. 1. Concordia diagram showing the MUN 02123 and Mt. Ste. Hilliare analysis and the ages weighted mean $^{206}Pb/^{238}U$ ages recorded. Error elipses are shown at 1σ and ages are calculated at 2σ.

in the argon gas causes an isobaric interference on ^{204}Pb. This makes the measurement of ^{204}Pb in zircon impossible with the instrumentation used in this study. To measure and correct for common-Pb present in the zircon we used the $^{208}Pb/^{206}Pb$–$^{232}Th/^{238}U$ method (Compston et al., 1984), which is quite commonly applied to zircon data collected using the SHRIMP (Williams, 1998 and Refs. therein). The analytical procedure for perovskite was essentially identical to zircon measurements, as was the data reduction, except for common-Pb corrections which are discussed below.

2.3. Common-Pb corrections

Compared to monazite or zircon, perovskite has low (U+Th)/Pb ratios and high (initial) common-Pb contents. This makes dating the mineral difficult particularly in the late Paleozoic–Cenozoic age ranges typically associated with many carbonatite and (diamond-bearing) kimberlite intrusions worldwide. It is therefore essential that common-Pb corrections can be made in order for accurate ages to be determined.

The most convenient way of expressing the amount of common-Pb is to define it as a fraction of total Pb in the mineral. The ^{204}Pb isotope is non-radiogenic and thus, the fraction of common-Pb can be expressed as:

$$f = {}^{204}\mathrm{Pb}/{}^{206}\mathrm{Pb}(\mathrm{measured})/{}^{204}\mathrm{Pb}/{}^{206}\mathrm{Pb}(\mathrm{common}) \quad (1)$$

The common-Pb corrected (radiogenic) ratio is then calculated using:

$$^{206}\mathrm{Pb}/{}^{238}\mathrm{U}(\mathrm{corrected}) = (1-f) * {}^{206}\mathrm{Pb}/{}^{238}\mathrm{U}(\mathrm{measured}). \quad (2)$$

Unfortunately, high Hg-backgrounds from the Ar plasma on many ICP-MS instruments cause an interference of ^{204}Hg on ^{204}Pb, which limits the use of this correction method.

The ^{208}Pb–^{206}Pb ratio is directly proportional to the ^{232}Th–^{238}U ratio and the age of the mineral. Minerals with high common-Pb contents will have ^{208}Pb–^{206}Pb ratios proportionately higher than their Th–Pb and U–Pb ratios and ages would predict. The ^{232}Th–$^{238}U/^{208}Pb$–^{206}Pb method (Compston et al., 1984) is used to estimate the expected radiogenic $^{208}Pb/^{206}Pb$ ratio where;

$$^{208}\mathrm{Pb}/{}^{206}\mathrm{Pb}\ (\mathrm{radiogenic}) = \frac{^{232}\mathrm{Th}}{^{238}\mathrm{U}} * \frac{(e^{\lambda}_{232^t} - 1)}{(e^{\lambda}_{238^t} - 1)} \quad (3)$$

The fraction of common-Pb is then calculated from;

$$f = ({}^{208}\mathrm{Pb}/{}^{206}\mathrm{Pb}(\mathrm{measured}) - {}^{208}\mathrm{Pb}/{}^{206}\mathrm{Pb}(\mathrm{radiogenic})) / (({}^{208}\mathrm{Pb}/{}^{206}\mathrm{Pb}(\mathrm{common}) - {}^{208}\mathrm{Pb}/{}^{206}\mathrm{Pb}(\mathrm{radiogenic})) \quad (4)$$

Table 2
LA-ICP-MS data for the Oka perovskite

Analysis #	Laser conditions			Calculated ratios							Common Pb content and corrected ratios			Apparent ages (Ma)	
	LAM power (mJ/p)	Spot size (μm)	Raster size (μm × μm)	Th/U	$^{206}Pb/^{238}U$	+/−	$^{207}Pb/^{206}Pb$	+/−	$^{238}U/^{206}Pb$	% err	f 206%	$*^{206}Pb/^{238}U$	+/−	$^{206}Pb/^{238}U$	+/−
mr15c07 1	0.5	20	80×30	2.87	0.0452	0.0026	0.4885	0.0186	22.14	5.82	59	0.0184	0.0021	118	16
mr15c08 1	0.5	20	80×30	2.23	0.0439	0.0024	0.4545	0.0152	22.78	5.51	55	0.0199	0.0022	127	17
mr15c09 1	0.5	20	80×30	3.29	0.0402	0.0021	0.4201	0.0172	24.86	5.25	50	0.0201	0.0024	129	17
mr15c10 1	0.5	20	80×30	2.18	0.0441	0.0021	0.4333	0.0184	22.69	4.65	52	0.0213	0.0025	136	17
mr27a09 1	0.5	15	60×45	2.10	0.0494	0.0025	0.4143	0.0277	20.24	5.10	49	0.0251	0.0036	160	20
mr30a05 1	0.5	15	100×80	2.56	0.0480	0.0029	0.4939	0.0225	20.82	6.01	60	0.0193	0.0023	123	17
mr30a06 1	0.5	15	100×80	2.55	0.0463	0.0022	0.4642	0.0186	21.61	4.67	56	0.0204	0.0024	130	16
mr30a07 1	0.5	15	100×80	3.44	0.0446	0.0025	0.4000	0.0173	22.44	5.55	47	0.0235	0.0028	150	20
mr30a08 1	0.5	15	100×80	2.50	0.0427	0.0043	0.4996	0.0276	23.43	10.17	61	0.0168	0.0022	107	19
mr30a09 1	0.5	15	100×80	3.91	0.0565	0.0028	0.5324	0.0220	17.71	4.97	65	0.0197	0.0023	126	16
mr30a10 1	0.5	15	100×80	2.76	0.0433	0.0032	0.4558	0.0311	23.11	7.29	55	0.0196	0.0028	125	19
ap02a04 1	0.5	20	60×60	4.30	0.0544	0.0046	0.5012	0.0247	18.38	8.49	61	0.0213	0.0027	136	22
ap02a05 1	0.5	20	60×60	2.58	0.0489	0.0026	0.4606	0.0233	20.44	5.30	55	0.0218	0.0028	139	18
ap02a06 1	0.5	20	60×60	2.79	0.0467	0.0022	0.4545	0.0285	21.39	4.67	55	0.0212	0.0029	136	17
ap02a07 1	0.5	20	60×60	2.65	0.0443	0.0028	0.4790	0.0277	22.56	6.36	58	0.0187	0.0025	119	17
ap02a08 1	0.5	20	60×60	3.44	0.0487	0.0022	0.4520	0.0205	20.54	4.56	54	0.0223	0.0027	142	17
ap02a09 1	0.5	20	60×60	4.63	0.0595	0.0027	0.5204	0.0202	16.81	4.56	63	0.0217	0.0025	139	17
ap02a11 1	0.5	20	60×60	2.73	0.0497	0.0022	0.4856	0.0165	20.13	4.39	59	0.0205	0.0023	131	16
ap02a12 1	0.5	10	60×60	2.65	0.0454	0.0021	0.4745	0.0168	22.02	4.63	57	0.0194	0.0022	124	15
ap02a13 1	0.5	10	30×30	2.40	0.0458	0.0017	0.4373	0.0205	21.83	3.70	52	0.0219	0.0027	140	16
ap02a14 1	0.5	10	30×30	2.73	0.0440	0.0040	0.4479	0.0210	22.75	9.21	54	0.0203	0.0025	130	22
ap02a15 1	0.5	10	30×30	4.07	0.0525	0.0035	0.4857	0.0242	19.06	6.66	59	0.0216	0.0027	138	20
ap02a16 1	0.5	10	30×30	4.09	0.0537	0.0040	0.5119	0.0195	18.62	7.45	62	0.0202	0.0023	129	19
ap02a17 1	0.5	10	40×40	2.55	0.0573	0.0029	0.4823	0.0197	17.45	5.01	58	0.0239	0.0028	152	19
ap02a18 1	0.5	10	40×40	2.73	0.0448	0.0029	0.4959	0.0230	22.34	6.43	60	0.0178	0.0022	114	16

$*^{206}Pb/^{238}U$ = radiogenic Pb/U ratio, i.e. corrected for common Pb. All errors and apparent ages quoted at the 1σ level.

The common-Pb corrected U/Pb ratio is then calculated using formula (2).

Perovskite commonly has high Th–U ratios, which means that even very high common-Pb contents cannot be reliably determined using this method (Compston et al., 1984; Williams, 1998). The correction methods in formulas (2) and (4) above rely on an assumed common-Pb ratio commonly based on a Pb-evolution model (e.g. Cumming and Richards, 1975; Stacey and Kramers, 1975). Thus, even if the Hg-interference can be overcome using on line gas filters or cleaner Ar-gas sources or perovskite with low Th/U ratio are targeted for analysis, corrections which rely on model Pb-compositions will be complicated by chemical interactions between the magma, source region and lithospheric components during emplacement which of course will be extreme in kimberlites. In other words the initial (common)-Pb ratios recorded by perovskite may differ significantly from simple model-Pb evolution values. Corrections could theoretically be made using the ^{208}Pb–^{206}Pb and/or ^{206}Pb–^{204}Pb ratios of common-Pb rich minerals coexisting with perovskite. However, suitable phases such as mica, feldspar and sulfide minerals are commonly altered and also occur as xenocrysts and therefore may not have the same common-Pb ratio as the magmatic perovskite.

A third method, which uses the measured $^{207}Pb/^{206}Pb$ ratio to estimate the common-Pb fraction, can be applied to U–Pb data. This method involves projecting a line through the uncorrected data on a Tera–Wasserburg plot and determining a common-Pb intercept on the $^{207}Pb/^{206}Pb$ axis. The $^{207}Pb/^{206}Pb$ value is then used as the basis for calculating the proportion of common-Pb (f) for each individual analysis by substituting the $^{207}Pb/^{206}Pb$ ratios for $^{208}Pb/^{206}Pb$ ratios in formula (4). The proportion of common-Pb is then subtracted from the measured $^{206}Pb/^{238}U$ ratio using formula (3). This correction is only employed in U–Pb dating of zircon and monazite in geologically young terranes (e.g. Ireland and Gibson, 1998) as determining the radiogenic $^{207}Pb/^{206}Pb$ ratio is the main objective in dating much of the geologic timescale. On the other hand, the range of radiogenic $^{207}Pb/^{206}Pb$ ratios for the Phanerozoic is relatively small (0.0461–0.0584) and the $^{206}Pb/^{238}U$ ratio is a more sensitive indicator of age for low-U

minerals, which have low radiogenic ^{207}Pb contents. The assumptions made when using the $^{207}Pb/^{206}Pb$ ratio to correct the $^{206}Pb/^{238}U$ ratio for common-Pb are that the mineral is concordant, and does not contain mixed age components. Given the fact that perovskite does not record inherited ages, and the main objective is to date the emplacement of rapidly cooled igneous rocks, these assumptions are likely to be valid in most cases. The correction has been in applied in dating perovskite (Kinney et al., 1997; Williams, 1998). We therefore have applied the $^{207}Pb/^{206}Pb$ correction method to each LA-ICP-MS pervoskite analysis in this study. The common-Pb corrected $^{206}Pb/^{238}U$ ratios were then used to calculate an age for each individual analysis and the weighted mean of several ages utilized to calculate the final age of the Oka perovskite crystals.

An alternative common-Pb correction, essentially a three dimensional correction which combines the data from ^{208}Pb, ^{206}Pb, ^{232}Th and ^{238}U, has recently been described in detail (Andersen, 2002). The method is mathematically quite complex and requires accurate measurement of $^{208}Pb/^{232}Th$ and $^{206}Pb/^{238}U$ and $^{232}Th/^{238}U$ ratios. Although in practice this is possible using the methodology in this study, standards with independent, accurate determination of $^{208}Pb/^{232}Th$ and $^{232}Th/^{238}U$ ratios are essentially non-existent, Furthermore, these values are not available

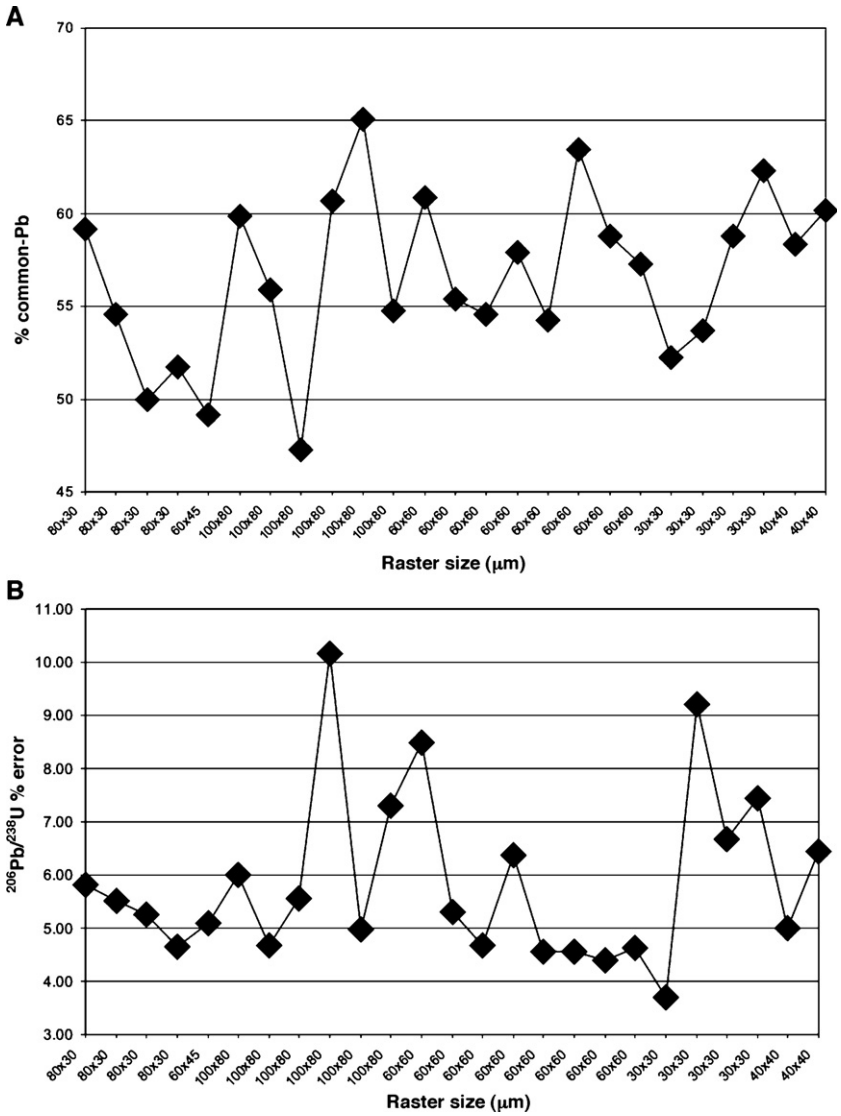

Fig. 2. Graphs showing each raster size against A) apparent common-Pb correction and (B) % error in corrected $^{206}Pb/^{238}U$ age (1σ). Note that despite that fact that larger raster areas sample a greater volume of the sample surface there is no apparent correlation with the common-Pb content, or correlation in errors with the smaller rasters.

for our 02123 reference zircon. We have chosen to focus on the use of a $^{207}Pb/^{206}Pb$ common Pb correction which essentially requires only the measurement of the $^{207}Pb/^{206}Pb$ and $^{206}Pb/^{238}Pb$ ratios and should be readily applicable in most LA-ICP-MS facilities.

2.4. Results from 02123 and Mt. Ste. Hilliare zircon analyses

The zircon reference data are presented in Table 1 and Fig. 1. U–Th–Pb ratios for zircon were corrected for common-Pb using the Stacey and Kramers (1975) model for Pb evolution and ages were calculated using the decay constants of Steiger and Jager (1977). The ages and the concordia diagrams were produced using the Isoplot/Ex macro (Ludwig, 2000) in conjunction with the LAMdate Excel spreadsheet program (Kosler et al., 2002). Corrected LA $^{206}Pb/^{238}U$ ratios for the 02123 zircon measurements ($N=16$), taken over the coarse of this study, gave a weighted mean value of 0.04616±0.00063, MSWD=0.79, which correspond to an age 291+/− 4 (values expressed at the 95% confidence interval). This is in close agreement with the accepted age of 295+/− 1 Ma (Ketchum et al., 2001).

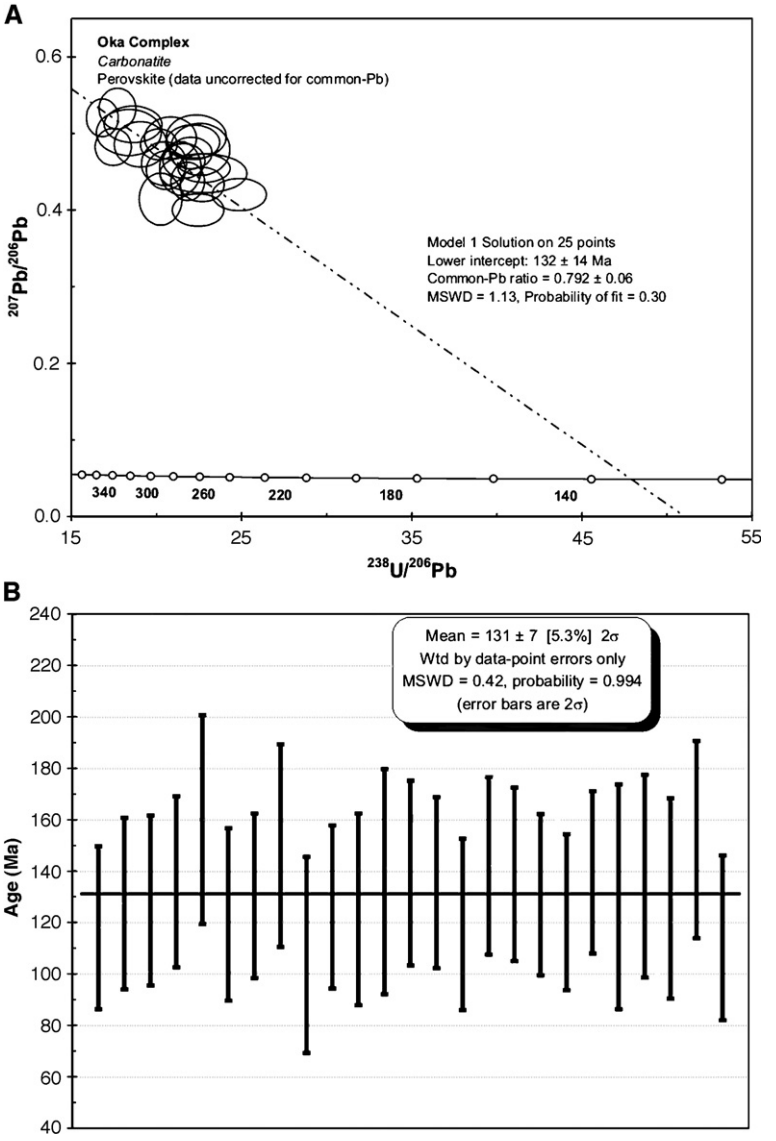

Fig. 3. (A) Tera–Wasserburg plot showing the uncorrected U–Pb data from the Oka perovskite. The intercepts represent the initial (common) $^{207}Pb/^{206}Pb$ ratio and the average $^{206}Pb/^{238}U$ age recorded by the data. Errors are shown at 1σ. (B) Weighted mean age based on based on all 25 common-Pb corrected $^{206}Pb/^{238}U$ ratios. Errors are shown and calculated at the 2σ level.

There is currently no independent age for the Mt. Ste. Hilliare zircon, but the accepted age for this complex is ca. 130–150 Ma based on the dating of lamprophyre intrusions from the same regional locality (Heaman and Kjarsgaard, 2000; Heaman and LeCheminant, 2001). As this is also in the same general locality of the Oka Complex, the analysis of the Mt. Ste. Hilliare zircon also allows for a check on the accuracy of the corrections applied to the perovskite data. Using the same set of correction parameters as applied to the 02123 zircon, the corrected LA data ($N=10$) for the Mte. Ste. Hilliare zircon gave a weighted mean $^{206}Pb/^{238}U$ ratio of 0.02210± 0.00082, MSWD=1.3, which corresponds to an age of 141+/− 7 Ma (values expressed at the 95% confidence interval). This age is in the range predicted for this sample and thus, we assumed that the experimental procedures were robust were applied to perovskite.

2.5. Ages from the Oka perovskite

The perovskite data, presented in Table 2 and Figs. 2–4, were reduced in the same way as the zircon data

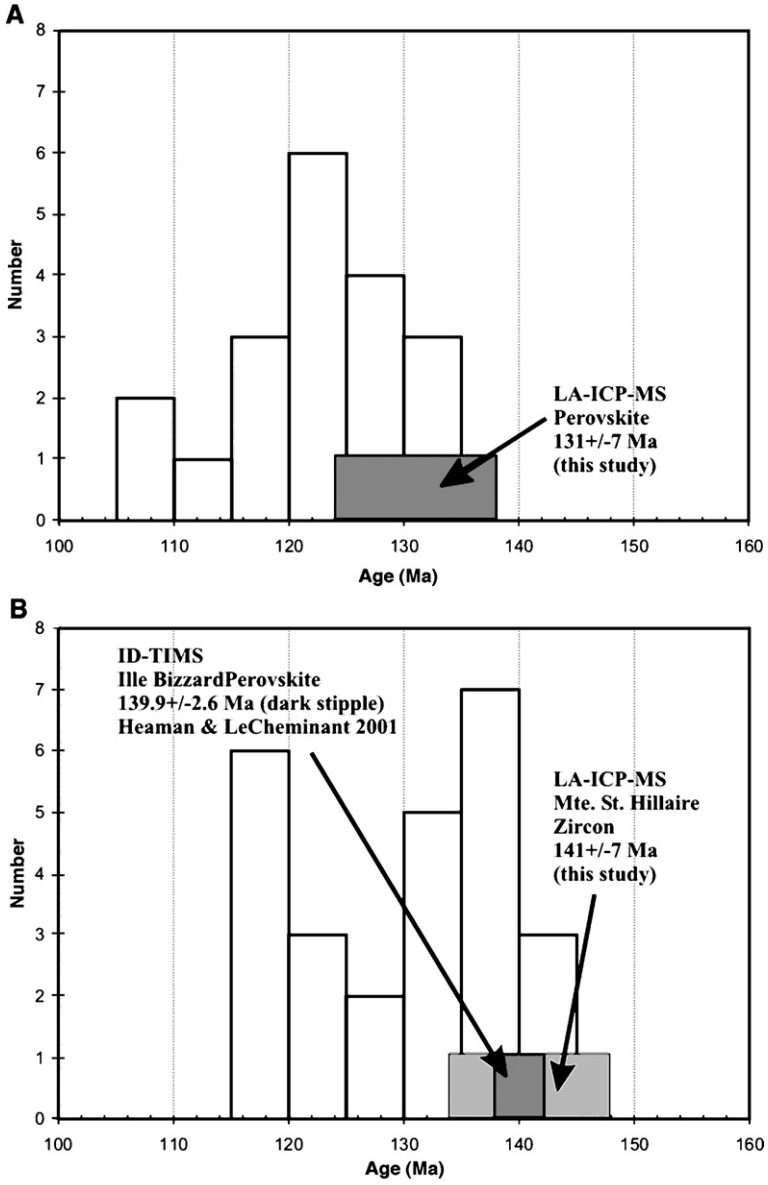

Fig. 4. Histogram showing the range of ages (excluding U–Pb ages) for (A) the Oka Complex and (B) nearby Monteregian intrusions. Data is shown in Table 3. The U–Pb ages are shown as separate stippled boxes. All ages are quoted at the 2σ level.

Table 3
Ages for the Oka Complex and nearby Monteregian intrusions (excluding U–Pb dates)

Intrusion	Rock type/ phase	Mineral dated	Method	Age	+/−	Ref
Oka	Not known	Biotite/ whole-rock	Rb–Sr	109	2	1
	Okaite	Apatite	Fission track	118	4	2
	Apatite Okaite	Apatite	Fission track	118	6	2
	Okaite	Apatite	Fission track	122	2	2
	Ijolite	Apatite	Fission track	121	2	2
	Ijolite	Apatite	Fission track	123	2	2
	Fo-Cpx-sovite	Apatite	Fission track	133	11	2
	Cpx-Pyr-sovite	Apatite	Fission track	126	6	2
	Cpx-Pyr-sovite	Apatite	Fission track	112	5	2
	Mel-Nio-sovite	Apatite	Fission track	108	8	2
	Mel-Nio-sovite	Apatite	Fission track	125	4	2
	Mont-Per-sovite	Apatite	Fission track	130	2	2
	Cpx-Bt-Pyr-sovite	Apatite	Fission track	125	18	2
	Cpx-Bt-sovite	Apatite	Fission track	124	7	2
	Mont-Pyr-sovite	Apatite	Fission track	132	4	2
	Mont-sovite	Apatite	Fission track	126	8	2
	Alnoite	Apatite	Fission track	119	12	2
	Alnoite	Apatite	Fission track	122	11	2
	Alnoite	Apatite	Fission track	121	12	2
Royal	Nepheline diorite	Sphene	Fission track	117	3	3
	Leucogabbro	Apatite	Fission track	138	6	3
	Pyroxenite	Apatite	Fission track	134	9	3
Bruno	Gabbro	Apatite	Fission track	135	11	3
	Pyroxenite	Apatite	Fission track	135	11	3
Johnson	Essexite	Apatite	Fission track	117	9	3
	Pulaskite	Apatite	Fission track	120	8	3
Rougemont	Gabbro	Apatite	Fission track	136	10	3
	Pyroxenite	Apatite	Fission track	138	11	3
Yamaska	Essexite	Apatite	Fission track	119	8	3
	Nepheline syenite	Sphene	Fission track	120	10	3
	Younger pyroxenite	Apatite	Fission track	132	10	3
	Older pyroxenite	Apatite	Fission track	140	9	3
	Gabbro	Apatite	Fission track	140	11	3
	Gabbro	Apatite	Fission track	141	9	3
Shefford	Nordmarkite	Whole-rock isochron	Rb–Sr	120.3	1	3
	Pulaskite	Whole-rock isochron	Rb–Sr	128.5	3	3
	Nepheline diorite	Apatite	Fission track	119	8	3
	Diorite	Apatite	Fission track	131	8	3
Brome	Nepheline diorite	Whole-rock isochron	Rb–Sr	118.4	2.2	3
	Pulaskite	Whole-rock isochron	Rb–Sr	136.2	1.7	3
	Nepheline diorite	Apatite	Fission track	117	9	3
	Gabbro	Apatite	Fission track	139	13	3
Megantic	Granite	Whole-rock isochron	Rb–Sr	127.6	1.7	3
	Nordmarkite	Whole-rock isochron	Rb–Sr	132.5	1.1	3
	Gabbro	Apatite	Fission track	134	8	3

The data were taken from (1) Wen et al. (1987), (2) Gold et al. (1986) and (3) Eby (1984) and are quoted at 2σ.

with additional calculations to determine individual common-Pb corrected ages. The first feature of the data is the relatively small spread in isotopic ratios. For example, the $^{238}U/^{206}Pb$ ratios in Kinney et al. (1997) range from about 6 to almost 20, compared to values ranging from 16.89 to 24.89 in this study. There is no apparent correlation between the volume of the crystal ablated (raster and spot size) and the measured isotopic ratio, or the overall precision of the analysis. Analysis were performed the same time (200 s) and with the same laser power (0.5 mj/pulse). Therefore analysis carried out over larger raster areas, with the smaller (15 μm) spot sizes will sample higher volumes of surface material than those carried out using a 10 μm spot size and 30×30 or 40×40 μm rasters. Common-Pb resulting from surface contamination would result in the former ablation analysis recording much lower $^{238}U/^{206}Pb$

ratios. The lack of any correlation between raster size and the $^{206}Pb/^{238}U$ ratio (Fig. 2A), however, indicates that surface contamination is not the cause of observed isotopic variations.

Smaller spot and raster sizes might be expected to cause significantly higher degrees of inter-elemental fractionation between U and Pb, which would result in lower $^{238}U/^{206}Pb$ ratios. In addition, after correction of residual fractionation using the linear intercept method, higher correction factors required for data from smaller rasters would lead in larger errors on calculated ratios (Kosler et al., 2002; Cox et al., 2003). However, as illustrated in Fig. 2B, this is not the case for the Oka perovskite data. A number of the smaller spot sizes and smaller raster areas in fact give the most precise analyses. Thus, variation in raster area and spot size, does not result in significant increases in fractionation. In addition, the lower volume of material supplied by smaller spot sizes, results in lower count rates for each measured mass. Again, this does not appear to cause significant decreases in the overall precision. In conclusion, the variation in the isotopic ratios is a reflection of different common-Pb contents within the analyzed volumes of perovskite. The relatively small variation in this case suggests similar U and common-Pb contents in both of the two large crystals analyzed. This represents the main limitation in accurately determining the $^{207}Pb/^{206}Pb$ intercept value which is subsequently used to correct each analysis for common-Pb. The data, uncorrected for common-Pb, are shown on a Tera–Waserburg plot in Fig. 3A at the 1σ level. The Model 1 solution (Ludwig, 1991) for these data gives a $^{207}Pb/^{206}Pb$ (common-Pb) intercept value of 0.792+/− 0.06 (MSWD=1.13, probability of fit=0.30) and an apparent $^{206}Pb/^{238}U$ age of 132+/− 14 Ma. The common-Pb $^{207}Pb/^{206}Pb$ value of 0.792+/− 0.06 is identical to a value of 0.79227+/− 0.0003 obtained on mineral separates by Grünenfelder et al. (1986). This further supports the conclusions that the use of the $^{207}Pb/^{206}Pb$ common Pb intercept value is a perfectly valid way of determining the final ages. Using the $^{207}Pb/^{206}Pb$ intercept value for the common-Pb composition, we are able to correct each individual analysis for initial-Pb. Common-Pb contents are consistently high, varying from 47% to 65% and this results in a significant propagation in the errors following common-Pb corrections. However, the individual common-Pb corrected $^{206}Pb/^{238}U$ ages show strong correlation at the 2σ interval and give a weighted mean age, calculated using Isoplot (Ludwig, 2000) of 131+/−7 Ma (MSWD=0.42, probability of fit=0.994). The strong concordance between this age, the intercept age indicated on the Tera–Wasserburg plot (Fig. 3B) and the common-Pb value from previous studies (Grünenfelder et al., 1986) suggests that the data were adequately corrected using the same common-Pb and that individual areas have not been affected by significant Pb-loss. Thus, 131+/− 7 Ma most likely represents the crystallization age for this phase of the Oka complex.

3. Discussion

The age ranges for the alkali-carbonatite Monteregian intrusives and the Oka complex in particular are highly varied (e.g. Eby, 1984; Gold et al., 1986). It is important to note that all but one age in the region has been determined using fission-track dating, Rb–Sr whole-rock isochron dating or K–Ar dating (e.g. Eby, 1984; Gold et al., 1986; Wen et al., 1987). It is widely accepted that the closure temperatures for these systems are significantly lower (80–350 °C) than for minerals dated using the U–Pb system including perovskite. The K–Ar ages from the Oka Complex have also largely been discounted due to excess Ar (see Wen et al., 1987). Given the history of multiple intrusions in the Oka complex it is unlikely that any of these lower temperature systems would be used in more modern studies to date multiple intrusive events. Despite this, if we take the all the available age data for the Oka Complex and nearby Monteregian intrusions (Table 3) it is clear that two age groups can be identified (Fig. 4). These two age groups 110–125 Ma and 125–140 Ma are largely the same as those identified by Eby (1984). The LA-ICP-MS age determined on perovskite in this study (131+/− 7 Ma) suggests that the montecellite–perovskite–sövite dated in this study belongs to the older phase of igneous activity in the region. This is consistent with not only the field relationships, but in fact is the same as the fission-track apatite age (130+/− 2 Ma) determined on the same rock (Gold et al., 1986).

The only high-precision ID-TIMS U–Pb age so far determined from the region is from the Ille Bizzard alnoite intrusion located some 10 km east of the Oka Complex. The age of 139.9+/− 2.6 Ma (Heaman and LeCheminant, 2001) for this intrusion is within error of the Oka perovskite sample dated in this study. This strongly suggests that the age determined by the LA-ICP-MS, using the $^{207}Pb/^{206}Pb$ correction method to account for common-Pb in the perovskite. This is further supported by the identical values for common-Pb determined in this study with those determined by Grünenfelder et al. (1986). Although is would clearly be desirable to have a concordant, high-U perovskite as a reference material, it also appears that with stable instrument conditions, and carefully applied correction procedures, zircon can been used as an interim reference material, despite the obvious matrix differences

between the two phases. The samples from the Oka carbonatite appear to have a relatively small spread in U–Pb ratios, no doubt as a result of a relatively homogeneous U-distribution. Despite this, the age obtained using the weighted mean of 25 analyses is sufficiently precise to be used to solve many geologic problems such as the timing of perovskite-bearing magma emplacement. The smallest raster used was 30×30 μm, creating a pit 10–15 μm deep. These analyses gave similar precision compared with larger raster sizes. The lowest volumes of sampled material, using the smallest rasters, should allow the technique to be applied to dating other rock-types such as kimberlite, where the average grain-size of matrix perovskite crystals is significantly smaller (~ 50 μm) than those studied here.

Finally, the LA-ICP-MS zircon age (141+/− 7 Ma) for the Monteregian Mte. Ste. Hillaire intrusion (Table. 1 and Figs. 1 and 4) also lies in the older age group. We suggest that a thorough investigation of these intrusions, using robust U–Pb dating of refractory minerals, would reveal that the majority of Rb–Sr and fission track ages represent reset and/or mixed ages caused by multiple phases of intrusive activity. A modern U–Pb dating study of the Monteregian intrusions is clearly required.

4. Conclusions

The low-cost and relative speed with which this type of age determination can be performed should make the LA-ICP-MS method an attractive alternative to ID-TIMS and SHRIMP where reconnaissance dating, rapid sample turn-around or a large number of ages are required. With careful calibration the general method may be readily adapted to dating methods used in most LA-ICP-MS labs. The only requirement for producing an accurate age is careful determination of the $^{207}Pb/^{206}Pb$ and $^{206}Pb/^{238}U$ ratios. Although we demonstrate that zircon can be used a calibration material for perovskite analyses, increased availability of matrix matched reference materials will undoubtedly assist in developing the LA-ICP-MS dating method and increase it's applicability to other minerals. We predict that a future study of ages recorded by rocks in the Monteregian alkaline igneous province, using robust U–Pb dating techniques, will reveal than emplacement ages will be older than those currently sited.

Acknowledgements

RAC gratefully acknowledges the support of Dr. Toby Rivers and Dr. Joe Hodych through their NSERC grants while employed as a PDRF at Memorial University. R.A.C was also supported in part by the DHCW's NSERC Grant during the course of this study. We would also like to acknowledge the highly constructive comments supplied by the two anonymous reviewers and by the editor Dr. Roberta Rudnick.

References

Andersen, T., 2002. Correction of common lead in U–Pb analyses that do not report ^{204}Pb. Chem. Geol. 192, 59–79.

Armstrong, R.A., Moore, R.O., 1998. Rb–Sr ages on kimberlites from the Lac de Gras area, Northwest Territories, Canada. S. Afr. J. Geol. 101, 155–158.

Ballard, J.R., Palin, J.M., Williams, I.S., Campbell, I.H., Faunes, A., 2001. Two ages of porphyry intrusion resolved for the super-giant Chuquicamata copper deposit of northern Chile by ELA-ICP-MS and SHRIMP. Geology 29, 383–386.

Belousova, E.A., Griffin, W.L., Shee, S.R., Jackson, S.E., O'Reilly, S.Y., 2001. Two age populations of zircons from the Timber Creek kimberlites, Northern Territory, as determined by laser-ablation ICP-MS analysis. Aust. J. Earth Sci. 48, 757–765.

Compston, W., Williams, I.S., Meyer, C.E., 1984. U–Pb geochronology of zircons from lunar breccia 73217 using a sensitive high mass-resolution ion microprobe. J. Geophys. Res. B89, 525–534.

Cox, R.A., Wilton, D.H.C., Kosler, J., 2003. Laser-ablation U–Th–Pb in situ dating of zircon and allanite; an example from the October Harbour Granite, central coastal Labrador, Canada. Can. Mineral. 41, 273–291.

Cumming, G.L., Richards, J.R., 1975. Ore lead isotope ratios in a continuously changing Earth. Earth Planet. Sci. Lett. 28, 155–171.

Davis, W.J., 1997. U–Pb zircon and rutile ages from granulite xenoliths in the Slave Province; evidence for mafic magmatism in the lower crust coincident with Proterozoic dike swarms. Geology 25, 343–346.

Davis, W.J., Kjarsgaard, B.A., 1997. A Rb–Sr isochron age for a kimberlite from the recently discovered Lac de Gras Field, Slave Province, Northwest Canada. J. Geol. 105, 503–509.

Eby, G.N., 1984. Geochronology of the Monteregian Hills alkaline igneous province. Québec. Geology 12, 468–470.

Feng, R., Machado, N., Ludden, J., 1993. Lead geochronology of zircon by laserprobe-inductively coupled plasma mass spectrometry (LP-ICPMS). Geochim. Cosmochim. Acta 57, 3479–3486.

Foster, G., Gibson, H.D., Parrish, R., Horstwood, M., Fraser, J., Tindle, A., 2002. Textural, chemical and isotopic insights into the nature and behaviour of metamorphic monazite. Chem. Geol. 191, 183–207.

Fryer, B.J., Jackson, S.E, Longerich, H.P., 1993. The application of laser ablation microprobe-inductively coupled plasma-mass spectrometry (LA-ICP-MS) to in situ (U)–Pb geochronology. Chem. Geol. 109, 1–8.

Gold, D.P., Eby, G.N., Bell, K., Vallée, M., 1986. Carbonatites, diatremes and ultra-alkaline rocks in the Oka area, Québec. GAC Guideb. 21.

Grünenfelder, M., Tilton, G.R., Bell, K., Blenkinsop, J., 1986. Lead and strontium isotope relationships in the Oka carbonatite complex, Quebec. Geochim. Cosmochim. Acta 50, 461–468.

Heaman, L.M., Kjarsgaard, B.A., 2000. Timing of eastern North American kimberlite magmatism; continental extension of the Great Meteor Hotspot track? Earth. Planet. Sci. Lett. 178, 253–268.

Heaman, L.M., LeCheminant, A.N., 2001. Anomalous U–Pb systematics in mantle-derived baddeleyite xenocrysts from Ile Bizard; evidence for high temperature radon diffusion? Chem. Geol. 172, 77–93.

Heaman, L.M, Creaser, R.A., Cookenboo, H.O., 2002. Extreme enrichment of high field strength elements in Jericho eclogite xenoliths; a cryptic record of Paleoproterozoic subduction, partial melting, and metasomatism beneath the Slave Craton, Canada. Geology 30 (6), 507–510.

Hodych, J.P., Cox, R.A., Kosler, J., 2004. An equatorial Laurentia at 550 Ma confirmed by Grenvillian inherited zircons dated by LA ICP-MS in the Skinner Cove volcanics of western Newfoundland: implications for inertial interchange true polar wander. Precambrian Res. 129, 93–113.

Horn, I., Rudnick, R.L., McDonough, W.F., 2000. Precise elemental and isotope ratio determination by simultaneous solution nebulization and laser ablation-ICP-MS; application to U–Pb geochronology. Chem. Geol. 164, 281–301.

Ireland, T.R., Gibson, G.M., 1998. SHRIMP monazite and zircon geochronology of high-grade metamorphism in New Zealand. J. Metamorph. Geol. 16, 149–167.

Kelley, S.P., Wartho, J.A., 2000. Rapid kimberlite ascent and the significance of Ar–Ar ages in xenolith phlogopites. Science. 289, 609–611.

Ketchum, J.W.F., Jackson, S.E., Culshaw, N.G., Barr, S.M., 2001. Depositional and tectonic setting of the Paleoproterozoic Lower Aillik Group, Makkovik Province, Canada: evolution of a passive margin-foredeep sequence based on petrochemistry and U–Pb (TIMS and LAM-ICP-MS) geochronology. Precambrian Res. 105, 331–356.

Kinney, P.D., Griffin, B.J., Heaman, L.M., Brakhfogel, F.F., Spetsius, Z.V., 1997. SHRIMP U–Pb ages of perovskite from Yakutian kimberlites. Russ. Geol. Geophys. 38, 97–105.

Kosler, J., Fonneland, H., Sylvester, P., Tubrett, M., Pedersen, R.B., 2002. U–Pb dating of detrital zircons for sediment provenance studies; a comparison of laser ablation ICPMS and SIMS techniques. Chem. Geol. 182, 605–618.

Leckie, D.A., Kjarsgaard, B.A., Bloch, J., McIntyre, D., McNeil, D., Stasiuk, L.D., Heaman, L.M., 1997. Emplacement and reworking of Cretaceous, diamond-bearing, crater facies kimberlite of central Saskatchewan, Canada. Geol. Soc. Amer. Bull. 109, 1000–1020.

Li, Xianhua, Liang Xirong, Sun Min, Guan Hong, Malpas, J.G., 2001. Precise $^{206}Pb/^{238}U$ age determination on zircons by laser ablation microprobe-inductively coupled plasma-mass spectrometry using continuous linear ablation. Chem. Geol. 175, 209–219.

Ludwig, K.R, 1991. ISOPLOT; a plotting and regression program for radiogenic-isotope data; version 2.53. U. S. Geological Survey Open File Report 09-0445.

Ludwig, K.R. 2000. ISOPLOT EX version 2.3. Berkeley Geochronological Centre Spec. Pub. No. 1a.

Machado, N., Gauthier, G., 1996. Determination of $^{207}Pb/^{206}Pb$ ages on zircon and monazite by laser-ablation ICPMS and application to a study of sedimentary provenance and metamorphism in southeastern Brazil. Geochim. Cosmochim. Acta 60, 5063–5073.

Machado, N., Simonetti, A., 2001. U–Pb dating and Hf isotopic composition of zircon by laser ablation-MC-ICP-MS. In: Sylvester, P.J. (Ed.), Laser-ablation-ICPMS in the Earth Sciences; Principles and Applications. MAC Short Course Handbook, vol. 29, pp. 121–146.

Phillips, D., Machin, K.J., Kiviets, G.B., Fourie, L.F., Roberts, M.A., Skinner, E.M.W., 1998. A petrographic and $^{40}Ar/^{39}Ar$ geochronological study of the Voorspoed Kimberlite, South Africa; implications for the origin of Group II kimberlite magmatism. S. Afr. J. Geol. 101, 299–306.

Queen, M., Heaman, L.M., Hanes, J.A., Archibald, D.A., Farrar, E., 1996. $^{40}Ar/^{39}Ar$ phlogopite and U–Pb perovskite dating of lamprophyre dykes from the eastern Lake Superior region; evidence for a 1.14 Ga magmatic precursor to Midcontinent Rift volcanism. Can. J. Earth Sci. 33, 958–965.

Schaerer, U., Corfu, F., Demaiffe, D., 1997. U–Pb and Lu–Hf isotopes in baddeleyite and zircon megacrysts from the Mbuji–Mayi Kimberlite; constraints on the subcontinental mantle. Chem. Geol. 143, 1–16.

Schmitz, M.D., Bowring, S.A., 2001. The significance of U–Pb zircon dates in lower crustal xenoliths from the southwestern margin of the Kaapvaal Craton, Southern Africa. Chem. Geol. 172, 59–76.

Scott, D.J., 1999. U–Pb geochronology of the eastern Hall Peninsula, southern Baffin Island, Canada; a northern link between the Archean of West Greenland and the Paleoproterozoic Torngat Orogen of northern Labrador. Precambrain Res. 93, 5–26.

Smith, C.B., Clark, T.C., Barton, E.S., Bristow, J.W., 1994. Emplacement ages of kimberlite occurrences in the Prieska region, southwest border of the Kaapvaal Craton, South Africa. Chem. Geol. 113, 149–169.

Spetsius, Z.V., Belousova, E.A., Griffin, W.L., O'Reilly, S.Y., Pearson, N.J., 2002. Archean sulfide inclusions in Paleozoic zircon megacrysts from the Mir Kimberlite, Yakutia; implications for the dating of diamonds. Earth Planet. Sci. Lett. 199, 111–126.

Stacey, J.S., Kramers, J.D., 1975. Approximation of terrestrial lead isotope evolution by two stage model. Earth Planet. Sci. Lett. 26, 207–211.

Steiger, R.H., Jager, E., 1977. Subcommision on geochronology: Convention on the use of decay constants in geo-and cosmochronology. Earth Panet. Sci. Lett. 36, 359–362.

Wen, J., Bell, K., Blenkinsop, J., 1987. Nd and Sr isotope systematics of the Oka Complex, Quebec, and their bearing on the evolution of the sub-continental upper mantle. Contrib. Mineral. Petrol. 97, 433–437.

White, N.M., Parrish, R.R., Bickle, M.J., Najman, Y.M.R., Burbank, D., Maithani, A., 2001. Metamorphism and exhumation of the NW Himalaya constrained by U–Th–Pb analyses of detrital monazite grains from early foreland basin sediments. J. Geol. Soc. Lond. 158, 625–635.

Williams, I.S., 1998. U–Th–Pb geochronology by ion microprobe. In: McKibben, M.A., Shanks, W.C., Ridley, W.I. (Eds.), Applications of Microanalytical Techniques to Understanding Mineralization Processes. SEG Rev. in Economic Geol., vol. 7, pp. 1–35.

Willigers, B.J.A., Baker, J.A., Krogstad, E.J., Peate, D.W., 2002. Precise and accurate in situ Pb–Pb dating of apatite, monazite, and sphene by laser ablation multiple-collector ICP-MS. Geochim. Cosmochim. Acta 66, 1051–1066.